Equilibrium and kinetics studies for the adsorption of Ni^{2+} and Fe^{3+} ions from aqueous solution by graphene oxide

Wojciech Konicki[1*], Małgorzata Aleksandrzak[2], Ewa Mijowska[2]

[1]*Maritime University of Szczecin, Department of Integrated Transport Technology and Environmental Protection, Henryka Pobożnego St. 11, 70-507 Szczecin, Poland*
[2]*West Pomeranian University of Technology, Szczecin, Faculty of Chemical Technology and Engineering, Institute of Chemical and Environment Engineering, Pułaskiego St. 10, 70-322 Szczecin, Poland*
[*]*Corresponding author: e-mail: w.konicki@am.szczecin.pl*

In this study, the adsorption of Ni^{2+} and Fe^{3+} metal ions from aqueous solutions onto graphene oxide (GO) have been explored. The effects of various experimental factors such as pH of the solution, initial metal ion concentration and temperature were evaluated. The kinetic, equilibrium and thermodynamic studies were also investigated. The adsorption rate data were analyzed using the pseudo-first-order kinetic model, the pseudo-second-order kinetic model and the intraparticle diffusion model. Kinetic studies indicate that the adsorption of both ions follows the pseudo-second-order kinetics. The isotherms of adsorption data were analyzed by adsorption isotherm models such as Langmuir and Freundlich. Equilibrium data fitted well with the Langmuir model. The maximum adsorption capacities of Ni^{2+} and Fe^{3+} onto GO were 35.6 and 27.3 mg g^{-1}, respectively. In addition, various thermodynamic parameters, such as enthalpy (ΔH^O), entropy (ΔS^O) and Gibbs free energy (ΔG^O), were calculated.

Keywords: nickel, iron, graphene oxide, adsorption, kinetics.

INTRODUCTION

Many industries such as mining, metallurgical, tannery, plumbing, textiles, electroplating, fertilizer, and battery manufacturing generate wastewater with various heavy metals. The release of wastewater from these industries to aquatic ecosystems may present an ecotoxic hazard. The heavy metals, even in traces, are not only toxic to living organisms in water, but also harmful effects to land animals including humans through food chain transfer. They are non-biodegradable and causing various diseases and disorders. Therefore, it becomes necessary to remove heavy metals from wastewaters before they are released into the environment. Several techniques have been used to remove heavy metals from industrial wastewater including chemical precipitation[1], coagulation[2], ion exchange[3], membrane filtration[4], reverse osmosis[5], electrolytic processes[6] and adsorption[7]. Among these methods, adsorption has been proved to be an efficient and economical technique.

The present study investigates the adsorption of Ni^{2+} and Fe^{3+} ions from aqueous solution. Nickel is a toxic heavy metal that is frequently used in many industrial processes such as metal plating, paint and pigment production, battery manufacture, galvanizing industries and mining. The higher concentration of nickel causes harmful effects like headache, dizziness, nausea, dry cough, tightness of the chest, vomiting, shortness of breath, cyanosis, chest pain, rapid respiration, cancer of lungs, nose and bone[8, 9]. Also iron is toxic at higher concentrations. Large quantities of wastewater containing various concentration of iron are generated from the iron and steel industry and mining. Iron toxicity lead to many problems like anorexia, oliguria, diarrhea, hypothermia, diphasic shock, metabolic acidosis and even death and it causes vascular congestion of the gastrointestinal tract, liver, kidneys, heart, brain, adrenals and thymus with acute iron poisoning much of the damage happens to the gastrointestinal tract and liver which results from the high level of iron concentration and free radical produc-tion leading to hepatotoxicity via lipid per oxidation and destruction of the hepatic mitochondria. As a result of iron storage disease, the liver becomes cirrhotic[10].

To date, many types of adsorbents have been tested for their ability to remove Ni^{2+} and Fe^{3+} ions from aqueous solutions. Hasar prepared activated carbon from almond husk by activating without and with H_2SO_4 at different temperatures for removal of Ni^{2+} ions[2]. Yang et al.[11] have investigated the adsorption of Ni^{2+} on oxidized multi--walled carbon nanotubes. Otun et al.[12] used powdered egg shell as adsorbent for removal of Ni^{2+} from aqueous solution. Rao et al.[13] have investigated the removal of Ni^{2+} from aqueous solution using bagasse and fly ash. Fiol et al.[14] have studied the adsorption of Ni^{2+} from aqueous solution by olive stone waste. Oztas et al.[15] have investigated the removal of Fe^{3+} ion from aqueous solution by adsorption on raw and treated clinoptilolite. Ravichandran and Arivoli[10] prepared activated calcite powder for removal of Fe^{3+} from aqueous solution. Hashemian et al.[16] have synthesized by hydrothermal process Linde Type-A zeolite as adsorbent for the re-moval of Fe^{3+} from aqueous solution. Bhattacharyya and Gupta[17] have studied the adsorption of Fe^{3+} from water by natural and acid activated clays. Li et al.[18] have investigated the removal of high-concentration Fe^{3+} by oxidized multiwall carbon nanotubes.

The aim of the present work was to study the efficiency of graphene oxide, as adsorbent to remove toxic heavy metal ions (Ni^{2+} and Fe^{3+}) from aqueous solutions. The effects of main parameters, i.e., initial solution pH, initial metal ion concentration, and solution temperature, were studied for ions removal. The equilibrium and kinetic data of adsorption studies were modeled using three kinetic models (pseudo-first-order, pseudo-second-order and intraparticle diffusion model) and two isotherm models (Langmuir and Freundlich). Thermodynamic parameters, such as enthalpy (ΔH^o), entropy (ΔS^o) and Gibbs free energy (ΔG^o), were also calculated.

EXPERIMENTAL

Material and characterization methods

Analytical grade standard solutions of 1000 mg L^{-1} Ni^{2+} ($Ni(NO_3)_2$) and Fe^{3+} ($Fe(NO_3)_3$) were purchased from Merck (Darmstadt, Germany). Dimethylglyoxime was obtained from Fluka (Buchs, Switzerland). 1,10-phenanthroline was obtained from Chempur (Poland).

Graphene oxide was prepared with modified Hummers method according to Marcano et al.[19]. Briefly, concentrated sulfuric acid and orthophosphoric acid (60:7.5 mL) were added to a mixture of $KMnO_4$ (3 g) and graphite (0.5 g). It was stirred for 24 h at 50°C. The resulting mixture was poured into ice (75 mL) and H_2O_2 (30%, 0.5 mL) and then centrifuged followed by washing with water, hydrochloric acid (30%) and ethanol. Finally, the GO was dried in air at 60°C.

The functional groups on the GO surface were determined using fourier transform infrared FTIR method (Nicolet iS5 FT-IR Spectrometer, Thermo Scientific). Thermogravimetric analysis (TGA), used to verify the content of oxygen functional groups in graphene oxide and its thermal stability, was carried out on a TA Instrument SDT Q600 under an air flow of 100 mL/min at heating rate of 10°C/min from room temperature to 800°C. Powder X-ray diffraction (XRD) of graphene oxide was recorded on a X'Pert Philips Diffractometer. The morphology of the obtained materials was characterized via atomic force microscopy (Nanoscope V MultiMode 8, Bruker). Raman spectra were acquired on the inVia Raman Microscope (Renishaw) at an excitation wavelength of 514 nm. The zeta potential of GO was determined by a Malvern Instrument Zetasizer 2000 at room temperature. All solutions were prepared with deionized water.

Adsorption experiments

Adsorption experiments were carried out in Erlenmeyer flask, where the solution (200 mL) with initial Ni^{2+} and Fe^{3+} concentration was placed. Initial concentrations of ions were varied from 5 to 25 mg L^{-1}. The experiments were conducted individually for Ni^{2+} and Fe^{3+}. The flask with ion solution was sealed and placed in a temperature controlled shaking water bath (Grant OLS26 Aqua Pro, Grant Instruments Ltd) and agitated at a constant speed of 160 rpm. To observe the effect of temperature the experiments were carried out at three different temperatures, i.e., 20, 40 and 60°C. Before mixing with the adsorbent, various pH of the solution was adjusted by adding a few drops of diluted hydrochloric acid (0.1 N HCl) or sodium hydroxide (0.1 N NaOH). When the desired temperature was reached, about 20 mg of GO was added into the flask. At predetermined moments, 1 ml of aqueous sample was taken from the solution, and the liquid was separated from the adsorbent by centrifugation at 6000 rpm for 5 min. The determination of Ni^{2+} and Fe^{3+} concentration was done spectrophotometrically (GENESYS 10S UV-VIS Spectrometer, Thermo Scientific) at 530 nm using the dimethylglyoxime method[20] and at 510 nm using the 1,10-phenanthroline method[21], respectively. The amount of ions adsorbed at time t q_t (mg g^{-1}) was calculated by following equation:

$$q_t = \frac{(C_0 - C_t)V}{m} \qquad (1)$$

where C_o (mg L^{-1}) is the initial ion concentration, C_t (mg L^{-1}) the ion concentration at any time t, V (L) the volume of the solution and m (g) is the mass of the adsorbent. Each experiment was performed two times and the results are given as average values. The kinetic and isotherm models were evaluated by the linear correlation coefficient (R^2).

RESULTS AND DISCUSSION

Characterization of the adsorbent

Figure 1 shows FTIR spectrum of GO. The peaks in the range of 950–1300 cm^{-1} indicate the presence of C-O bonds in various chemical surroundings[22]. The peak at 1402 cm^{-1} may be associated with H-O bending vibration in water, phenols and carboxyls[23]. The peak at 1589 cm^{-1} is attributed to C=C stretching mode of sp^2 carbon skeletal network[24]. The peak at 1726 cm^{-1} can be assigned to C=O stretching vibration in carboxyls or carbonyls[25]. The broad peak at 3403 cm^{-1} corresponds to O-H stretching vibration due to the existence of surface hydroxylic groups and chemisorbed water[26].
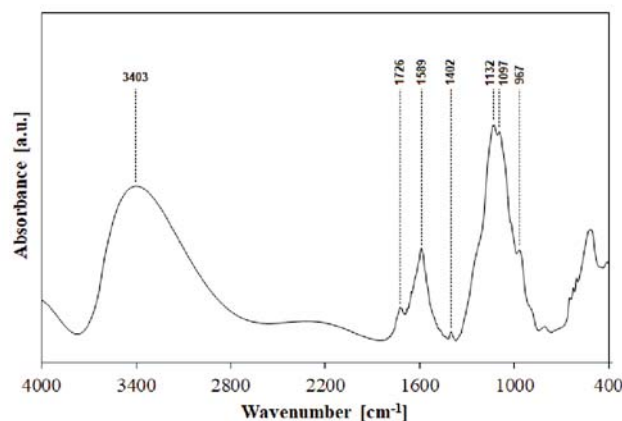

Figure 1. FTIR spectra of GO

Thermogravimetric analysis is further used to estimate the content of the oxygen-functional groups and thermal stability of graphene oxide (Fig. 2). It indicates that during heating in air ~34.7 wt.% of GO is removed in the temperature range of 160–250°C, due to release of oxygen-containing functional groups. Decomposition of carbon skeleton proceeded at roughly 400–700°C[27].

XRD pattern of graphene oxide is presented in Figure 3. The pattern demonstrates a sharp peak at 2θ of 11.19°, which corresponds to (001) reflection of graphene oxide and an interlayer distance of 0.79 nm. The increased d-spacing compared to graphite (0.34 nm) is a result of the intercalation of oxygen-containing functional groups and water molecules into graphene layers during the oxidation process[28].

Figure 4 presents topography and height profiles of graphene oxide measured with atomic force microscopy. The AFM analysis confirmed successful exfoliation of graphite leading to the formation of graphene oxide flakes. According to the height profiles, the thickness of graphene oxide is in the range of 0.77–2.94 nm. Basing
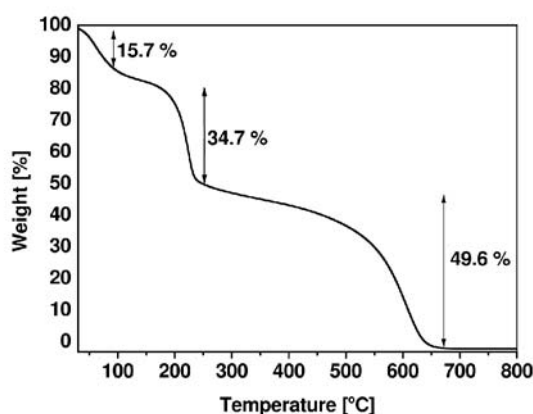
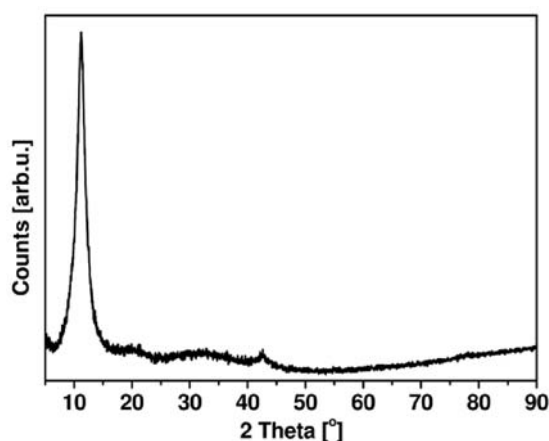**Figure 2.** Thermogravimetric curve of GO

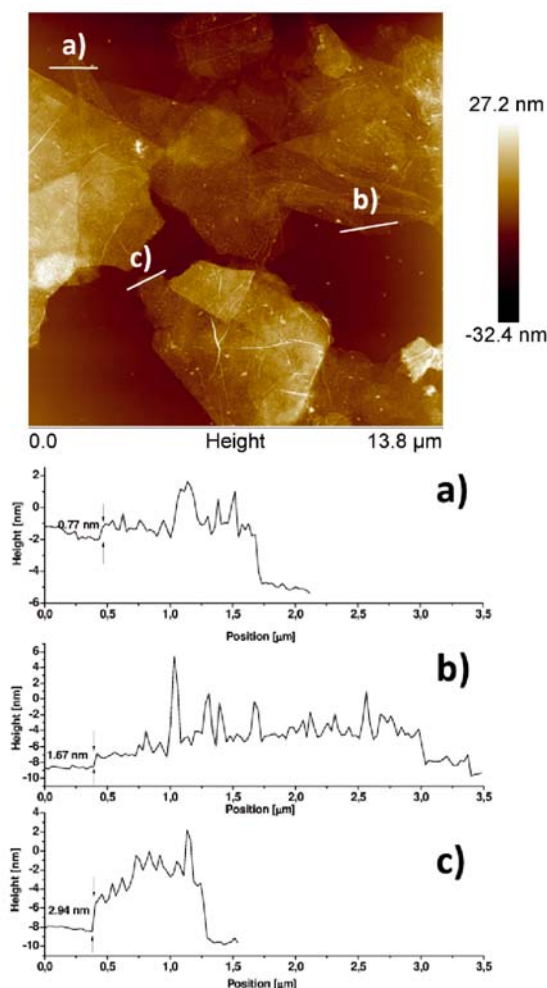**Figure 3.** XRD pattern of GO

Figure 4. AFM image and height profiles of GO

on the interlayer distance (0.79 nm), it is assumed that the obtained GO isa mixture of single-, bi- and few-layer graphene oxide.

Figure 5 presents typical Raman spectrum of graphene oxide measured with laser of 514 nm. It shows G band at 1604 cm^{-1} which corresponds to Raman allowed phonon mode at the center of the Brillouin zone with E_{2g} symmetry[29]. It is governed by a single resonance process and it is a common feature of all graphitic materials, however, the band is up-shifted in comparison to G band of graphite ($\sim$1580 cm^{-1}), which may be attributed to an isolated double bonds resonating at higher frequencies[30]. The D mode at 1353 cm^{-1} is a breathing mode of A_{1g} symmetry involving phonons near the K zone boundary. D mode is related to the defects in graphene and the intensity ratio of I_D/I_G can be used to characterize the level of disorder in graphene. Hence, the I_D/I_G was calculated to be 1.12. The I_D/I_G value indicates highly disordered graphite, which could arise from introduction of oxygen-containing fuctional groups to the graphite lattice. 2D band at 2701 cm^{-1} originates from a two phonon double resonance Raman process. The peak at 2940 cm^{-1}, which is the D+D' band, is the combination of phonons with different momenta around K and Γ, thus requiring a defect for its activation[31].

The zeta potentials of GO were measured at pH in the range 1.7–12.2, and the values were negative over the entire studied pH range, varying from –15.5 mV to –34.9 mV (Fig. 6).
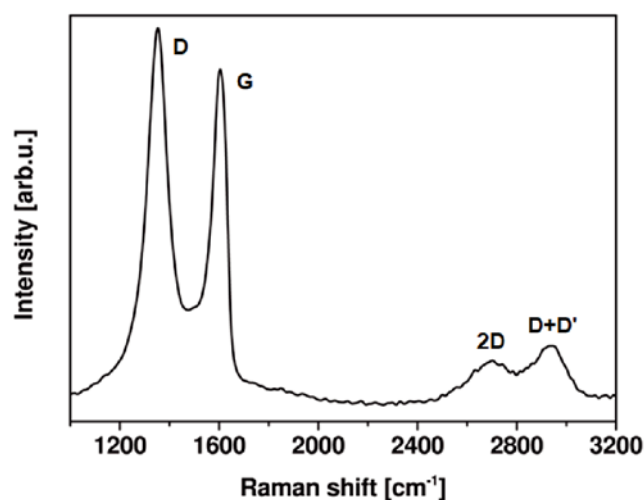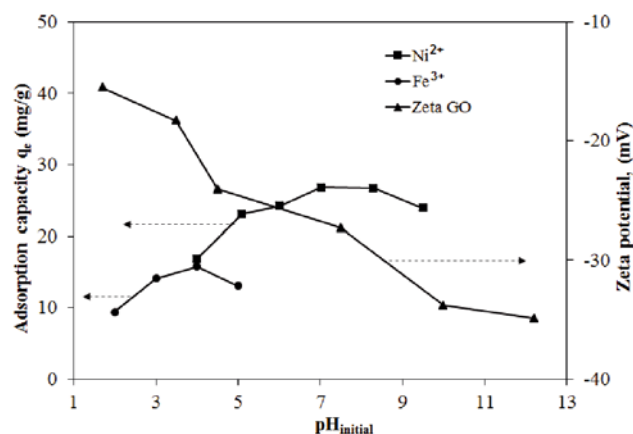

Figure 5. Raman spectrum of GO

Figure 6. The effect of initial pH solution on adsorption Ni^{2+} and Fe^{3+} onto GO (Experimental conditions: $C^o_{Ni(II) \text{ and } Fe(III)}$ = 10 mg L^{-1}, T = 20°C)

Effect of pH

One of the most important factors controlling the adsorption of metal ions is pH. The effect of the initial pH on the adsorption of Ni^{2+} and Fe^{3+} ions onto GO was studied in pH range from 2 to 9.5 at a fixed ions concentration of 10 mg L^{-1} and temperature of 20°C. However, for Fe^{3+} adsorption experiments were conducted from pH 2 to 5 in order to avoid the ions precipitation. The results are shown in Figure 6. Additionally, to understand the adsorption mechanism, it is necessary to determine the zeta potentials of the adsorbent at different pH values. Therefore, Figure 6 also shows the effect of the initial pH on zeta potentials of GO. When the initial pH was increased from 1.7 to 12.2, the zeta potential of GO decreased from –15.5 to –34.9 mV, and it was negative over the entire studied pH range. The surface of GO contains some oxygen groups such as carboxylic groups (R-COOH) and hydroxylic groups (R-OH).

At pH>pH$_{pzc}$ (point of zero charge of the adsorbent) these groups dissociate to anionic form (R-COO$^-$ and R-O$^-$), what increases the number of negatively charged sites and generates electrostatic attraction force with Ni^{2+} and Fe^{3+} ions. As seen in Figure 6, the adsorption capacity increased from 16.9 to 26.8 for Ni^{2+} and from 9.4 to 15.8 for Fe^{3+} when the pH increased from 4 to 7 and from 2 to 4, respectively. However, further increase of pH, the adsorption capacity of Ni^{2+} and Fe^{3+} ions decreased. The decrease in adsorption capacity of both ions is probably due to the formation of soluble hydroxy complexes. Nickel is presents in the species of Ni^{2+}, $Ni(OH)^+$, $Ni(OH)_2$, $Ni(OH)_3^-$ and $Ni(OH)_4^{2-}$ at different pH values[11]. At pH<9, the predominant form is Ni^{2+}. With the increase in pH, the concentration of Ni^{2+} ions decreases rapidly and increases the concentration of $Ni(OH)^+$, $Ni(OH)_2$ and $Ni(OH)_3^-$. As a result, the optimum pH for Ni^{2+} adsorption was found to be pH 7, therefore the other adsorption experiments were performed at this pH. Also, the concentration of dissolved Fe^{3+} decreases with increasing pH as Fe^{3+} solubility is limited by the precipitation of ferric hydroxides $Fe(OH)_3$ and oxyhydroxides $FeOOH$[32]. The precipitation of Fe^{3+} ions from solution was observed at pH values higher than 2.5[15, 17, 33, 34]. In our study, the maximum adsorption capacity of Fe^{3+} onto GO is at pH 4. Therefore, pH 4 was selected as the optimal for further experiments with Fe^{3+} ions.

Adsorption kinetics

The effect of initial ions concentration for the adsorption of Ni^{2+} and Fe^{3+} onto GO was investigated in the concentration range of 5–25 mg L^{-1} at 20°C (Fig. 7). It is evident from this figure that the amount of adsorbed ions increased from 18.9 to 31.7 mg g^{-1} for Ni^{2+} and from 11.1 to 21.9 mg g^{-1} for Fe^{3+}, with increasing the initial concentration of both ions.

The removal of Ni^{2+} and Fe^{3+} by adsorption on GO was found to be rapid at the initial period of contact time and then to slow down with increasing in contact time. The equilibrium was reached after 320 min for both ions.

Pseudo-first-order, pseudo-second-order and intraparticle diffusion models were applied to test the experimental data and thus elucidated the kinetic adsorption
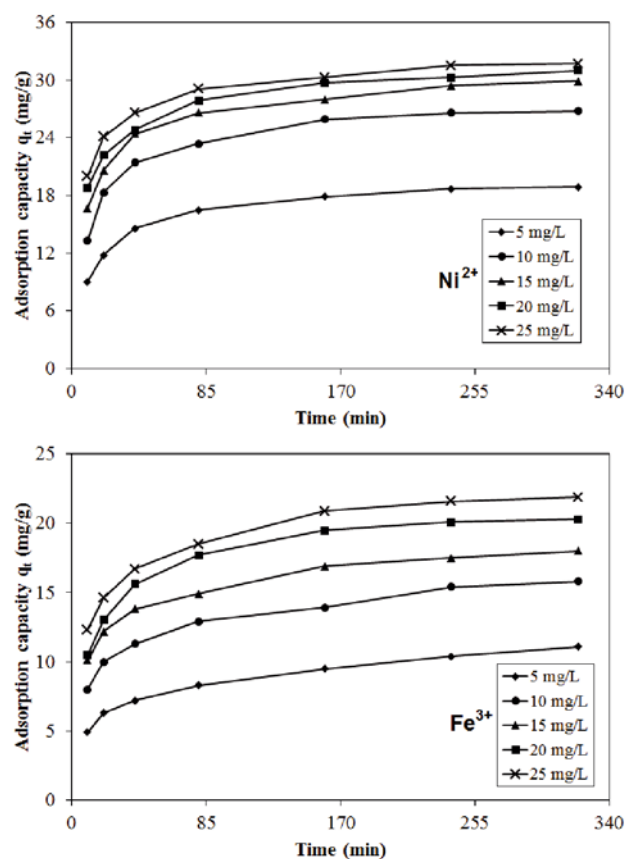

Figure 7. The effect of initial concentration of Ni^{2+} and Fe^{3+} on adsorption capacity onto GO

process of ions onto GO. The pseudo-first-order model is represented by the following equation[35]:

$$\ln(q_e - q_t) = ln q_e - k_1 t \qquad (2)$$

where q_e (mg g^{-1}) is the amount of ions adsorbed per unit mass of adsorbent at equilibrium, q_t (mg g^{-1}) is the amount of ions adsorbed per unit mass of adsorbent at any time t (min) and k_1 (min^{-1}) is the first-order rate constant adsorption. Values of k_1 and equilibrium adsorption density q_e were calculated from the plots of $\ln(q_e-q_t)$ versus t for different initial concentrations of ions.

The pseudo-second-order kinetic model can be expressed as follows:

$$\frac{t}{q_t} = \frac{1}{k_2 q_e^2} + \frac{1}{q_e} t \qquad (3)$$

where k_2 (g mg^{-1} min^{-1}) is the rate constant for the pseudo-second-order adsorption kinetics. Values of k_2 and q_e for different initial concentrations of ions were calculated from the slope and intercept of the linear plot of t/q_t versus t (Fig. 8). The results of the kinetic parameters for Ni^{2+} and Fe^{3+} adsorption are given in Table 1. Basing on the correlation coefficients R^2, the adsorption of both ions is best described by the pseudo-second-order kinetic model. A good agreement with this kinetic model is confirmed by the similar values of calculated adsorption capacity $q_{e,cal}$ and the experimental ones $q_{e,exp}$ for Ni^{2+} and Fe^{3+}. These results indicate that the adsorption of Ni^{2+} and Fe^{3+} onto GO belongs to the pseudo-second-order kinetic model.

Similar trends were observed for the adsorption of Ni^{2+} onto bael tree leaf powder[36], Cajanus cajan L Milsp seed shell activated carbons[37], oxidized multi-walled carbon

Table 1. Comparison of the pseudo-first-order, pseudo-second-order and the intraparticle diffusion models for different initial concentrations of Ni^{2+} and Fe^{3+}

Ion	C_o [mg L^{-1}]	$q_{e,exp}$ [mg g^{-1}]	Pseudo-first-order kinetic model			Pseudo-second-order kinetic model			Intraparticle diffusion model		
			k_1 [min^{-1}]	$q_{e,cal}$ [mg g^{-1}]	R^2	[g mg^{-1} min^{-1}]	$q_{e,cal}$ [mg g^{-1}]	R^2	k_p [mg g^{-1} $min^{-0.5}$]	C [mg g^{-1}]	R^2
Ni^{2+}	5	18.9	0.0169	11.7	0.9667	0.00258	19.7	0.9999	0.2758	14.21	0.9499
	10	26.8	0.0184	15.9	0.9723	0.00130	27.8	0.9998	0.3812	20.44	0.8796
	15	29.9	0.0144	15.0	0.9191	0.00106	30.7	0.9996	0.3832	23.21	0.9855
	20	31.0	0.0139	14.3	0.9012	0.00099	31.7	0.9997	0.3390	25.07	0.9667
	25	31.7	0.0176	14.9	0.9295	0.00095	32.4	0.9998	0.3073	26.43	0.9647
Fe^{3+}	5	11.1	0.0098	7.1	0.9377	0.00741	11.5	0.9949	0.3140	5.51	0.9995
	10	15.8	0.0126	9.6	0.9282	0.00372	16.4	0.9971	0.3440	9.77	0.9709
	15	18.0	0.0130	9.6	0.9321	0.00291	18.5	0.9989	0.3420	12.13	0.9374
	20	20.3	0.0174	12.3	0.9745	0.00224	21.1	0.9998	0.2924	15.38	0.9054
	25	21.9	0.0159	12.6	0.9653	0.00194	22.7	0.9994	0.3798	15.51	0.8997
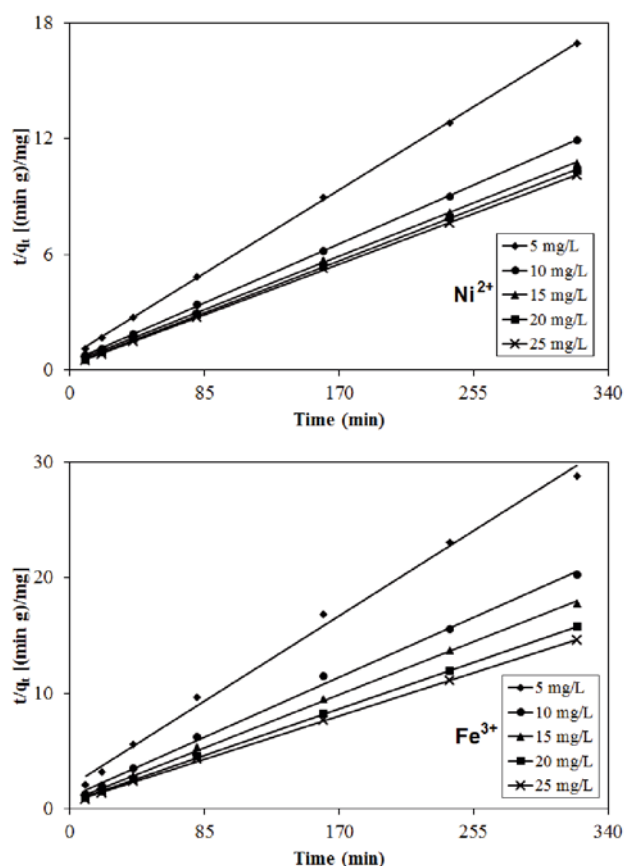
Figure 8. Pseudo-second-order kinetics of adsorption Ni^{2+} and Fe^{3+} onto GO at 20°C

nanotubes[11], and for the adsorption of Fe^{3+} onto chitosan and cross-linked chitosan beads[38], sand and charcoal mixture[39], zeolite[16] and nano copper oxide particles[40].
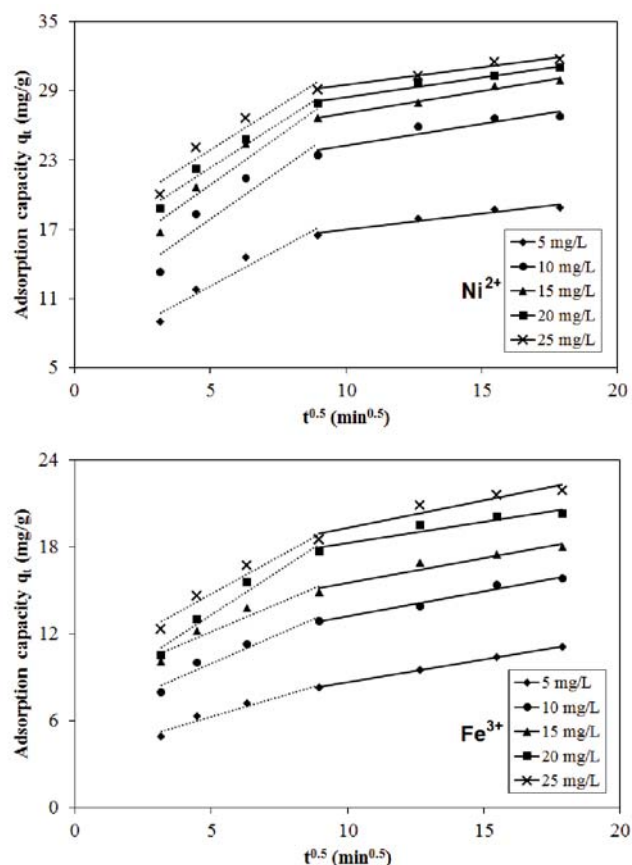
The intraparticle diffusion model was used to identify the diffusion mechanism during adsorption process. The intraparticle diffusion model is described by the following equation:

$$q_t = k_p t^{0.5} + C \tag{4}$$

where C (mg g^{-1}) is the constant which describes the boundary layer affects and k_p (mg g^{-1} $min^{-0.5}$) is the intraparticle diffusion rate constant, which was calculated from the slope of the linear plots of q_t versus $t^{0.5}$ (Fig. 9).

The plots present two different portions, indicating the different stages in adsorption. The first, sharper portion (dotted line) represents the external mass transfer. The second portion (solid line) is the gradual adsorption sta-

ge where intraparticle diffusion is rate-limiting. As can be seen from Figure 9, the lines do not pass through the origin, this indicates that the intraparticle diffusion is involved in the adsorption process but not the only rate-controlling step. The values of C are helpful in determining the boundary thickness: a larger C value corresponds to a greater boundary layer diffusion effect. The C values increased with the initial Ni^{2+} and Fe^{3+} concentration (Table 1). The results of this study demonstrated that increasing the initial ions concentrations promoted the boundary layer diffusion effect.

Figure 9. Intraparticle diffusion model of adsorption Ni^{2+} and Fe^{3+} onto GO at 20°C

Adsorption isotherms

The equilibrium adsorption models of Langmuir and Freundlich were used for the quantitative description of Ni^{2+} and Fe^{3+} uptake. The Langmuir model assumes monolayer coverage of adsorbate over a homogenous

adsorbent surface. The Freundlich model describes a heterogeneous adsorption surface and active sites with different energy. The linearized form of the Langmuir isotherm is expressed as follows[41]:

$$\frac{C_e}{q_e} = \frac{1}{Q_0 b} + \frac{C_e}{Q_0} \tag{5}$$

where Q_O (mg g^{-1}) is the monolayer adsorption capacity and b (L mg^{-1}) is a constant related to energy of adsorption. The values of Q_O and b were calculated from the slope and intercept of the linear plot C_e/q_e versus C_e (Fig. 10(a)). The essential characteristics of the Langmuir isotherm can be expressed in terms of a dimensionless equilibrium parameter (R_L), which is defined by the following equation:

$$R_L = \frac{1}{1 + bC_0} \tag{6}$$

where b (L mg^{-1}) is the Langmuir constant and C_o (mg L^{-1}) is the highest initial concentration of the adsorbate. The value of R_L indicates the type of the isotherm to be either unfavorable ($R_L > 1$), linear ($R_L = 1$), favorable ($0 < R_L < 1$) or irreversible ($R_L = 0$).

The linear form of Freundlich equation can be expressed as follows[42]:

$$\ln q_e = \ln K_F + \left(\frac{1}{n}\right) \ln C_e \tag{7}$$

where K_F (mg g^{-1}(L mg^{-1})$^{1/n}$) and n are Freundlich constants, which represent adsorption capacity and adsorption strength, respectively. The values of K_F and n were calculated from the slope and intercept of the linear plot ln q_e versus ln C_e (Fig. 10(b)). The value of n ranging from 1 to 10 indicated that the adsorption process is favourable.

The Langmuir and Freundlich constants and the linear correlation coefficients R^2 for both isotherms are listed in Table 2. It is found that the Langmuir model fit the data better than the Freundlich model, which indicates that the adsorption of Ni^{2+} and Fe^{3+} onto GO is a type of monolayer adsorption. Several authors have also reported this Langmuir-type adsorption behavior of ions onto such adsorbents as multiwall carbon nanotube/iron oxide magnetic composites[43] and activated carbon prepared from almond husk[9] for Ni^{2+} and raw and pretreated clinoptilolite[15], brown algae Sargassum Vulgare[34] or oxidized multiwall carbon nanotubes[18] for Fe^{3+}. The obtained values of R_L were found to be 0.092 and 0.196 for Ni^{2+} and Fe^{3+}, accordingly. These R_L values showed that the adsorption of both ions onto GO is a favorable process. The maximum adsorption capacities Q_O of GO for Ni^{2+} and Fe^{3+} calculated from Langmuir adsorption isotherm were 35.6 and 27.3 mg g^{-1}, respectively. Table 3 and 4 shows the comparison of the maximum monolayer adsorption capacities of various adsorbents for Ni^{2+} and Fe^{3+}.
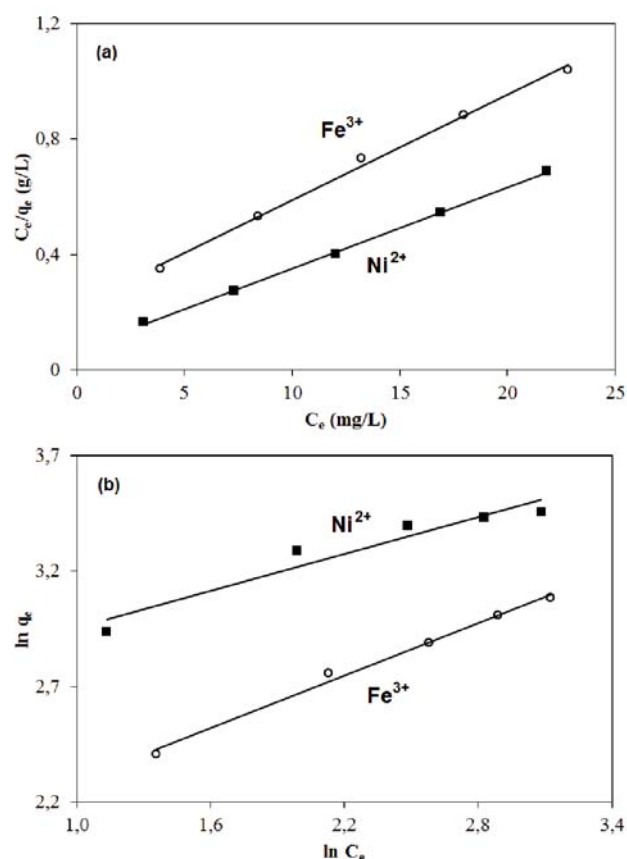

Figure 10. Langmuir (a) and Freundlich (b) adsorption isotherm of Ni^{2+} and Fe^{3+} onto GO at 20°C

Effect of temperature

The effect of temperature on the removal of Ni^{2+} and Fe^{3+} from aqueous solution by the GO was studied for three temperatures of 20, 40, and 60°C at 10 mg L^{-1}, and the results are presented in Figure 11. It can be observed that the adsorption capacity increase with the increases in temperature, from 26.8 to 30.1 mg g^{-1} for Ni^{2+}, and from 15.8 to 19.0 mg g^{-1} for Fe^{3+}, respectively.

The thermodynamic parameters such as enthalpy (ΔH^o), entropy (ΔS^o) and Gibbs free energy (ΔG^o), were determined by using the following equations:

$$\ln K_a = \frac{\Delta S^o}{R} - \frac{\Delta H^o}{R \cdot T} \tag{8}$$

where T (K) is the solution temperature, K_a is the adsorption equilibrium constant, R (8.314 J mol^{-1} K^{-1}) is the gas constant. Enthalpy (ΔH^o) and entropy (ΔS^o) were calculated from the slope and intercept of van't Hoff plot of ln q_e/C_e versus 1/T (Fig. 12). The value of Gibbs free energy (ΔG^o) was calculated using Eq. 10. The thermodynamic parameters were summarized in Table 5.

The positive ΔH^o values suggests that the adsorption process of both ions is endothermic. This can be explained by the phenomenon of hydration of heavy metal ions in water[63]. Since ions travel through solution and reach the adsorption sites, it is necessary for them to

Table 2. Langmuir and Freundlich parameters for the adsorption of the Ni^{2+} and Fe^{3+} onto GO at 20°C

Ion	Langmuir isotherm				Freundlich isotherm		
	Q_O [mg g^{-1}]	b [L mg^{-1}]	R_L	R^2	K_F [(mg g^{-1})(L mg^{-1})$^{1/n}$]	n	R^2
Ni^{2+}	35.6	0.396	0.092	0.9993	14.7	3.75	0.9306
Fe^{3+}	27.3	0.164	0.196	0.9959	6.75	2.63	0.9926

Table 3. Comparison of the maximum monolayer adsorption of Ni^{2+} onto various adsorbents

Adsorbent	Adsorbate	Q_O [mg g^{-1}]	Ref.
Bagasse	Ni^{2+}	0.001	13
Fly ash	Ni^{2+}	0.03	13
Aspergillus niger	Ni^{2+}	1.10	44
Oxidized CNTs	Ni^{2+}	1.83	45
Oxidized MWCNTs	Ni^{2+}	3.73	11
Rice hull	Ni^{2+}	5.75	46
Sheep manure waste	Ni^{2+}	7.20	47
Deactivated protanated yeast	Ni^{2+}	9.01	48
Peat moss	Ni^{2+}	9.18	49
Coir pith	Ni^{2+}	9.50	50
Fe_3O_4	Ni^{2+}	11.53	51
Carbon aerogel	Ni^{2+}	12.87	52
Zeolite/vermiculite composite	Ni^{2+}	16.50	53
Activated carbon prepared from almond husk	Ni^{2+}	30.77–37.18	9
GO	Ni^{2+}	35.6	This study
Granular activated carbon	Ni^{2+}	45.46–125.00	54
Graphene nanosheet/δ-MnO_2 composite	Ni^{2+}	46.55	55
Activated carbon-zeolite composite	Ni^{2+}	62.22–70.43	56
Cajanus cajan L Milsp seed shells activated carbon	Ni^{2+}	85.69–156.25	37
Lignocellulose/Montmorillonite nanocomposite	Ni^{2+}	94.86	57

Table 4. Comparison of the maximum monolayer adsorption of Fe^{3+} onto various adsorbents

Adsorbent	Adsorbate	Q_O [mg g^{-1}]	Ref.
E. coli biofilm supported on kaolin	Fe^{3+}	1.0–16.5	58
Activated Carbon from Recinius Communis Linn.	Fe^{3+}	1.181–1.569	59
Kaolinite	Fe^{3+}	11.2	17
Acid activated kaolinite	Fe^{3+}	12.1	17
Sand and charcoal mixture	Fe^{3+}	19.23	39
GO	Fe^{3+}	27.3	This study
Montmorillonite	Fe^{3+}	28.9	17
Acid activated montmorillonite	Fe^{3+}	30.0	17
Pretreated clinoptilolite	Fe^{3+}	44.8–104.0	15
Cross-linked chitosan beads	Fe^{3+}	46.30–72.46	38
Algae Sargassum Vulgare	Fe^{3+}	63.67	34
Cajanus cajan husk	Fe^{3+}	66.63	60
Thiourea Cross-Linked Chitosan	Fe^{3+}	71.9	61
Oxidized Multiwall Carbon Nanotubes	Fe^{3+}	89.05	18
Chitosan	Fe^{3+}	90.09	38
Raw clinoptilolite	Fe^{3+}	98.0	15
Activated Calcite Powder	Fe^{3+}	107.0–220.18	10
Plaster of Paris	Fe^{3+}	125.40–227.61	62
Copper oxide nano-particles	Fe^{3+}	126.32	40
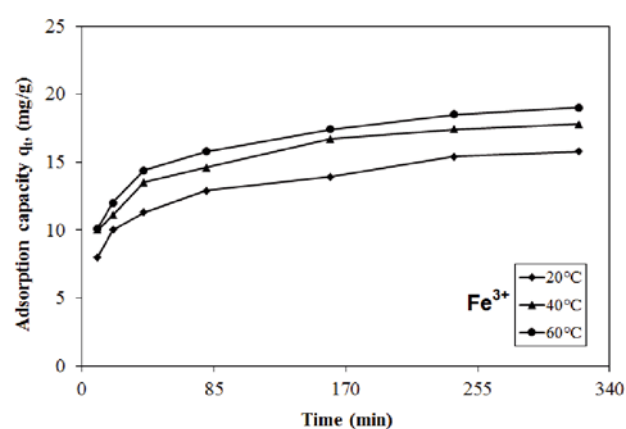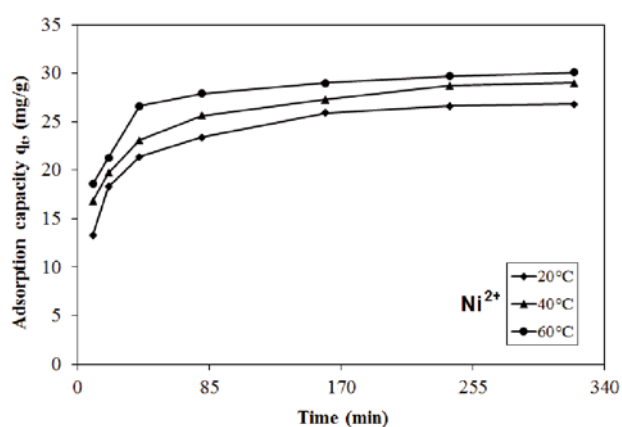
Figure 11. Effect of temperature on adsorption of the Ni^{2+} and Fe^{3+} onto GO

be stripped out of their hydration shell, that requires energy input. Thus, the positive value of ΔH^o indicates that the adsorption is increasing with temperature. A similar phenomenon was also reported previously for the adsorption of Cu^{2+}, Cd^{2+}, Zn^{2+} and Ni^{2+} ions onto MWCNTs/chitosan nanocomposite[64], Cu^{2+}, Pb^{2+} and Cd^{2+}

ions onto dithiocarbamated-spororpollenin[65], and for the adsorption of Pb^{2+} and Zn^{2+} ions onto termite mound[66].

The positive ΔS^o values suggested the increase in the degree of freedom at the solid-liquid interface mostly encountered in metal binding due to the release of water molecules of the hydration sphere during the adsorption

Table 5. Thermodynamic parameters for the adsorption of the Ni^{2+} and Fe^{3+} onto GO

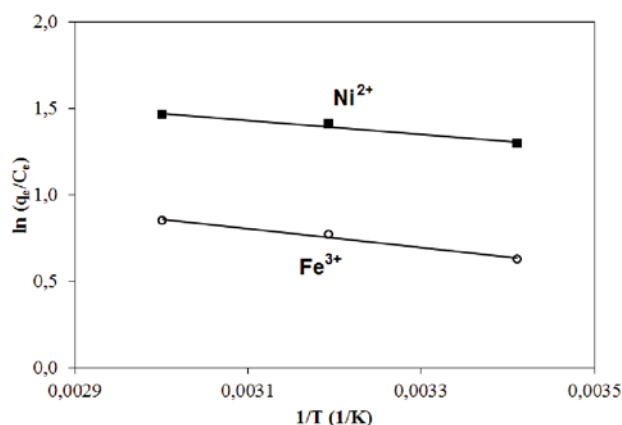| Ion	ΔH^O [kJ mol^{-1}]	ΔS^O [J mol^{-1} K^{-1}]	ΔG^O at temperature [^{O}C] [J mol^{-1}]		
Ni^{2+}	3.31	22.2	20	40	60
			−3.16	−3.66	−4.04
Fe^{3+}	4.55	20.8	20	40	60
			−1.53	−2.01	−2.36

Figure 12. Van't Hoff plot for the adsorption of the Ni^{2+} and Fe^{3+} onto GO

processes[67]. The values of ΔG^o for all tested temperatures were calculated to be negative, what suggests that the adsorption of Ni^{2+} and Fe^{3+} onto GO was spontaneous and thermodynamically favorable. Kara et al.[68] suggested that the ΔH^O of physisorption is smaller than 40 kJ mol^{-1}. Thus, the values of ΔH^o suggests that the adsorption of Ni^{2+} and Fe^{3+} onto GO is a physisorption process. Additionally, the values of ΔG^o between −20 and 0 kJ mol^{-1} indicate a physical adsorption process[69].

CONCLUSIONS

This work examined the efficiency of graphene oxide (GO) in removal of Ni^{2+} and Fe^{3+} ions from aqueous solution. The effects of adsorption parameters, such as initial pH, initial metal ion concentration and temperature, were studied. The adsorption of Ni^{2+} and Fe^{3+} ions was shown to be dependent on the initial pH solution, and the optimum pH values for the adsorption were 7.0 and 4.0 for Ni^{2+} and Fe^{3+}, respectively. Kinetic data were well fitted by a pseudo second-order kinetic model. The equilibrium adsorption data of both Ni^{2+} and Fe^{3+} onto GO were better fitted to Langmuir than Freundlich adsorption isotherm model. The maximum monolayer adsorption capacities were 35.6 mg g^{-1} and 27.3 mg g^{-1} for Ni^{2+} and Fe^{3+}, respectively. Thermodynamic parameters indicated that the adsorption of both ions onto GO was spontaneous and endothermic in nature. Additionally, the values of ΔH^o and ΔG^o suggested that the adsorption of Ni^{2+} and Fe^{3+} onto GO was a physisorption process. Therefore, we belive that GO is a suitable candidate for heavy metals ions removal, however the optimal pH should be defined prior the application.

LITERATURE CITED

1. Pang, F.M., Teng, S.P., Teng, T.T. & Mohd Omar, A.K. (2009). Heavy Metals Removal by Hydroxide Precipitation and Coagulation-Flocculation Methods from Aqueous Solutions. *Water Qual. Res. J. Can.* 44(2), 174–182.

2. Amuda, O., Amoo, I., Ipinmoroti, K. & Ajayi, O. (2006). Coagulation/flocculation process in the removal of trace metals present in industrial wastewater. *J. Appl. Sci. Environ. Mgt.* 10 (3), 159–162. http://dx.doi.org/10.4314/jasem.v10i3.17339

3. Vaaramaa, K. & Lehto, J. (2003). Removal of metals and anions from drinking water by ion exchange. *Desalination* 155, 157–170. DOI: 10.1016/S0011-9164(03)00293-5.

4. Blocher, C., Dorda, J., Mavrov, V., Chmiel, H., Lazaridis, N.K. & Matis, K.A. (2003). Hybrid flotation-membrane filtration process for the removal of heavy metal ions from wastewater. *Water Res.* 37, 4018–4026. http://dx.doi.org/10.1016/S0043-1354(03)00314-2

5. da Silva, J.R.P., Mercon, F., Costa, C.M.G. & Benjo, D.R. (2016). Application of reverse osmosis process associated with EDTA complexation for nickel and copper removal from wastewater. *Desalin. Water Treat.* 57(41), 19466–19474. http://dx.doi.org/10.1080/19443994.2015.1100554

6. Bertazzoli, R., Widner, R.C., Lanza, M.R.V., Di Iglia, R.A. & Sousa, M.F.B. (1997). Electrolytic Removal of Metals Using a Flow-Through Cell with a Reticulated Vitreous Carbon Cathode. *J. Braz. Chem. Soc.* 8(5), 487–493. http://dx.doi.org/10.1590/S0103-50531997000500009

7. Laus, R., Costa, T.G., Szpoganicz, B. & Favere, V.T. (2010). Adsorption and desorption of Cu(II), Cd(II) and Pb(II) ions using chitosan crosslinked with epichlorohydrin-triphosphate as the adsorbent. *J. Hazard. Mater.* 183, 233–241. http://dx.doi.org/10.1016/j.jhazmat.2010.07.016

8. Prabakaran, R. & Arivoli, S. (2012). Adsorption kinetics, equilibrium and thermodynamic studies of Nickel adsorption onto Thespesia Populnea bark as biosorbent from aqueous solutions. *Euro. J. Appl. Eng. Sci. Res.* 1(4), 134–142.

9. Hasar, H. (2003). Adsorption of nickel(II) from aqueous solution onto activated carbon prepared from almond husk. *J. Hazard. Mater.* B97, 49–57. DOI: 10.1016/s0304-3894(02)00237-6.

10. Ravichandran, T. & Arivoli, S. (2013). Adsorption of Fe (III) Ions by Activated Calcite Powder-Equilibrium, Kinetic and Thermodynamics Studies. *J. Pharm. Biomed. Res.* 2(1), 52–59.

11. Yang, S., Li, J., Shao, D., Hu, J. & Wang, X. (2009). Adsorption of Ni(II) on oxidized multi-walled carbon nanotubes: Effect of contact time, pH, foreign ions and PAA. *J. Hazard. Mater.* 166, 109–116. DOI: 10.1016/j.jhazmat.2008.11.003.

12. Otun, J.A., Oke, I.A., Olarinoye, N.O., Adie, D.B. & Okuofu, C.A. (2006). Adsorption isotherms of Pb(II), Ni(II) and Cd(II) ions onto PES. *J. Appl. Sci.* 6(11), 2368–2376. DOI: 10.3923/jas.2006.2368.2376.

13. Rao, M., Parwate, A.V. & Bhole, A.G. (2002). Removal of Cr^{6+} and Ni^{2+} from aqueous solution using bagasse and fly ash. *Waste Manage.* 22, 821–830. http://dx.doi.org/10.1016/S0956-053X(02)00011-9

14. Fiol, N., Villaescusa, I., Martinez, M., Miralles, N., Poch, J. & Serarols, J. (2006). Sorption of Pb(II), Ni(II), Cu(II) and Cd(II) from aqueous solution by olive stone waste. *Sep. Purif. Technol.* 50, 132–140. DOI: 10.1016/j.seppur.2005.11.016.

15. Öztaş, N.A., Karabakan, A. & Topal, Ö. (2008). Removal of Fe(III) ion from aqueous solution by adsorption on raw and treated clinoptilolite samples. *Micropor. Mesopor. Mat.* 111, 200–205. DOI: 10.1016/j.micromeso.2007.07.030.

16. Hashemian, S., Hosseini, S.H., Salehifar, H. & Salari, K. (2013). Adsorption of Fe(III) from Aqueous Solution by Linde Type-A Zeolite. *Am. J. Anal. Chem.* 4, 123–126. http://dx.doi.org/10.4236/ajac.2013.47A017

17. Bhattacharyya, K.G. & Gupta, S.S. (2006). Adsorption of Fe(III) from water by natural and acid activated clays: Studies on equilibrium isotherm, kinetics and thermodynamics of interactions. *Adsorption* 12, 185–204. DOI: 10.1007/s10450-006-0145-0.

18. Li, Y., Hu, X., Ren, B. & Wang, Z. (2016). Removal of High-Concentration Fe(III) by Oxidized Multiwall Carbon Nanotubes in a Fixed Bed Column. *Am. Chem. Sci. J.* 10(3), 1–9. DOI: 10.9734/ACSJ/2016/21692.

19. Marcano, D.C., Kosynkin, D.V., Berlin, J.M., Sinitskii, A., Sun, Z., Slesarev, A., Alemany, L.B., Lu, W. & Tour, J.M. (2010). Improved synthesis of graphene oxide. *ACS Nano* 4, 4806–4814. DOI: 10.1021/nn1006368.

20. Sykuła-Zając, A., Turek, M., Mathew, M.P., Patai, F., Horvat, M. & Jabłońska, J. (2010). Determination of nickel in tea by using dimethylglyoxime method. *Sci. Bull. Tech. Univ. Lodz. Food Chem. Biotechnol.* 74(1081), 5–11.

21. ISO 6332:1988. Water quality. Determination of iron. Spectrometric method using 1,10-phenanthroline.

22. Estévez-Martínez, Y., Velasco-Santos, C., Martínez-Hernández, A.L., Delgado, G., Cuevas-Yáńez, E., Alaníz-Lumbreras, D., Duron-Torres, S. & Castańo, V.M. (2013). Grafting of Multiwalled Carbon Nanotubes with Chicken Feather Keratin. *J. Nanomater.* 2013, 1–9. http://dx.doi.org/10.1155/2013/702157

23. Chen, J., Chen, Q., Ma, Q., Li, Y. & Zhu, Z. (2012). Chemical treatment of CNTs in acidic $KMnO_4$ solution and promoting effects on the corresponding Pd-Pt/CNTs catalyst. *J. Mol. Catal. A: Chem.* 356, 114–120. DOI: 10.1016/j.molcata.2011.12.032.

24. Kyzas, G.Z., Travlou, N.A., Kalogirou, O. & Deliyanni, E.A. (2013). Magnetic Graphene Oxide: Effect of Preparation Route on Reactive Black 5 Adsorption. *Materials* 6, 1360–1376. DOI: 10.3390/ma6041360.

25. Chen, J., Zhu, Z.H., Ma, Q., Li, L., Rudolph, V. & Lu, G.Q. (2009). Effects of pretreatment in air microwave plasma on the structure of CNTs and the activity of Ru/CNTs catalysts for ammonia decomposition. *Catal. Today* 148, 97–102. DOI: 10.1016/j.cattod.2009.02.005.

26. Li, Y., Du, Q., Liu, T., Peng, X., Wang, J., Sun, J., Wang, Y., Wu, S., Wang, Z., Xiaa, Y. & Xia, L. (2013). Comparative study of methylene blue dye adsorption onto activated carbon, graphene oxide, and carbon nanotubes. *Chem. Eng. Res. Des.* 91(2), 361–368. DOI: 10.1016/j.cherd.2012.07.007.

27. Stankovich, S., Dikin, D.A., Piner, R.D., Kohlhaas, K.A., Kleinhammes, A., Jia, Y., Wu, Y., Nguyen, S.B.T. & Ruoff, R.S. (2007). Synthesis of Graphene-Based Nanosheets via Chemical Reduction of Exfoliated Graphite Oxide. *Carbon* 45, 1558–1565. DOI: 10.1016/j.carbon.2007.02.034.

28. Some, S., Kim, Y., Yoon, Y., Yoo, H.J., Lee, S., Park, Y. & Lee, H. (2013). High-quality reduced graphene oxide by a dual-function chemical reduction and healing process. *Sci. Rep.* 3, 1–5. DOI: 10.1038/srep01929.

29. Couzi, M., Bruneel, J.-L., Talaga, D. & Bokobza, L. (2016). A multi wavelength Raman scattering study of defective graphitic carbon materials: The first order Raman spectra revisited. *Carbon* 107, 388–394. http://dx.doi.org/10.1016/j.carbon.2016.06.017

30. Kudin, K.N., Ozbas, B., Schniepp, H.C., Prud'homme, R.K., Aksay, I.A. & Car, R. (2008). Raman spectra of graphite oxide and functionalized graphene sheets. *Nano Lett.* 8(1), 36–41. DOI: 10.1021/nl071822y.

31. Iqbal, M.W., Singh, A.K., Iqbal, M.Z. & Eom, J. (2012). Raman fingerprint of doping due to metal adsorbates on graphene. *J. Phys. Condens. Matter.* 24, 335301–335307. DOI: 10.1088/0953-8984/24/33/335301.

32. Lottermoser, B.G. (2010). *Mine Wastes. Characterization, Treatment and Environmental Impacts*. Springer-Verlag, London, New York.

33. Vasu, A.E. (2008). Adsorption of Ni(II), Cu(II) and Fe(III) from Aqueous Solutions Using Activated Carbon. *E-J. Chem.* 5(1), 1–9. http://dx.doi.org/10.1155/2008/690241

34. Benaisa, S., El Mail, R. & Jbari, N. (2016). Biosorption of Fe (III) from aqueous solution using brown algae Sargassum Vulgare. *J. Mater. Environ. Sci.* 7(5), 1461–1468.

35. Chairat, M., Rattanaphani, S., Bremner, J.B. & Rattanaphani, V. (2008). Adsorption kinetic study of lac dyeing on cotton. *Dyes Pigm.* 76, 435–439. DOI: 10.1016/j.dyepig.2006.09.008.

36. Kumar, P.S. & Kirthika, K. (2009). Equilibrium and kinetic study of adsorption of nickel from aqueous solution onto bael tree leaf powder. *J. Eng. Sci. Technol.* 4(4), 351–363.

37. Thamilarasu, P., Sivakumar, P. & Karunakaran, K. (2011). Removal of Ni(II) from aqueous solutions by adsorption onto Cajanus cajan L Milsp seed shell activated carbons. *Indian J. Chem. Technol.* 18(5), 414–420.

38. Wan Ngah, W.S., Ab Ghani, S. & Kamari, A. (2005). Adsorption behaviour of Fe(II) and Fe(III) ions in aqueous solution on chitosan and cross-linked chitosan beads. *Bioresource Technol.* 96, 443–450. DOI: 10.1016/j.biortech.2004.05.022.

39. Deka, L. & Bhattacharyya, K.G. (2015). Batch adsorption studies for iron(III) removal from aqueous solution by sand and charcoal mixture. *J. Appl. Fund. Sci.* 1(1), 74–80.

40. Taman, R., Ossman, M.E., Mansour, M.S. & Farag, H.A. (2015). Metal Oxide Nano-particles as an Adsorbent for Removal of Heavy Metals. *J. Adv. Chem. Eng.* 5(3), 1–8. http://dx.doi.org/10.4172/2090-4568.1000125

41. Langmuir, I. (1918). The adsorption of gases on plane surfaces of glass, mica and platinum. *J. Am. Chem. Soc.* 40, 1361–1403.

42. Freundlich, H. (1906). Concerning adsorption in solutions. *Zeitschrift fur Physikalische Chemie* 57, 385–470.

43. Chen, C., Hu, J., Shao, D., Li, J. & Wang, X. (2009). Adsorption behavior of multiwall carbon nanotube/iron oxide magnetic composites for Ni(II) and Sr(II). *J. Hazard. Mater.* 164, 923–928. DOI: 10.1016/j.jhazmat.2008.08.089.

44. Kapoor, A. & Viraragavan, T. (1998). Heavy metal biosorption sites in Aspergillus Niger. *Bioresour. Technol.* 61, 221–227. http://dx.doi.org/10.1016/S0960-8524(97)00055-2

45. Gao, Z., Bandosz, T.J., Zhao, Z., Han, M. & Qiu, J. (2009). Investigation of factors affecting adsorption of transition metals on oxidized carbon nanotubes. *J. Hazard. Mater.* 167, 357–365. DOI: 10.1016/j.jhazmat.2009.01.050.

46. Suemitsu, R., Uenishi, R., Akashi, I. & Kakano, M. (1986). The use of dyestuff-treated rice hulls for removal of heavy metals from wastewater. *J. Appl. Polym. Sci.* 31, 75–83. DOI: 10.1002/app.1986.070310108.

47. Al-Rub, F.A.A., Kandah, M. & Aldabaibeh, N. (2002). Nickel removal from aqueous solution by using sheep Manure Waste. *Eng. Life Sci.* 2, 111–116. DOI: 10.1002/1618-2863(200204).

48. Padmavathy, V. (2008). Biosorption of Ni(II) ions on Baker's yeast: kinetic, thermodynamic and desorption studies. *Bioresour. Technol.* 99, 3100–3109. DOI: 10.1016/j.biortech.2007.05.070.

49. Ho, Y.S., Wase, D.A.J. & Forster, C.F. (1995). Batch nickel removal from aqueous solution by Sphagnum moss peat. *Water Res.* 29, 1327–1332. http://dx.doi.org/10.1016/0043-1354(94)00236-Z

50. Ewecharoen, A., Thiravetyan, P. & Nakbanpote, W. (2008). Comparison of nickel adsorption form electroplating rinse water by coir pith and modified coir pith. *Chem. Eng. J.* 137, 181–188. DOI: 10.1016/j.cej.2007.04.007.

51. Sharma, Y.C. & Srivastava, V. (2010). Separation of Ni(II) ions from aqueous solutions by magnetic nanoparticles. *J. Chem. Eng. Data* 55, 1441–1442. DOI: 10.1021/je900619d.

52. Meena, A.K., Mishra, G.K., Rai, P.K., Rajgopal, C. & Nagar, P.N. (2005). Removal of heavy metal ions from aqueous solution using carbon aerogel as an adsorbent. *J. Hazard. Mater.* 122, 161–170. DOI: 10.1016/j.jhazmat.2005.03.024.

53. Johnson, C.D. & Worrall, F. (2007). Novel granular materials with microcrystalline active surfaces-waste water treatment applications of zeolite/vermiculite composites. *Water Res.* 4, 2229–2235. http://dx.doi.org/10.1016/j.watres.2007.01.047

54. Kinhikar, V.R. (2012). Removal of Nickel (II) from Aqueous Solutions by Adsorption with Granular Activated Carbon (GAC). *Res. J. Chem. Sci.* 2(6), 6–11.

55. Yueming Ren, N.Y. (2011). Graphene/δ-MnO_2 composite as adsorbent for the removal of nickel ions from wastewater. *Chem. Eng. J.* 175, 1–7. http://dx.doi.org/10.1016/j.cej.2010.08.010

56. Jha, V.K., Matsuda, M. & Miyake, M. (2008). Sorption properties of the activated carbon-zeolite composite prepared from coal fly ash for Ni^{2+}, Cu^{2+}, Cd^{2+} and Pb^{2+}. *J. Hazard. Mater.* 160, 148–153. http://dx.doi.org/10.1016/j.jhazmat.2008.02.107

57. Zhang, X. & Wang, X. (2015). Adsorption and desorption of nickel(II) ions from aqueous solution by a lignocellulose/montmorillonite nanocomposite. *PLoS One* 10(2), 1–21. http://dx.doi.org/10.1371/journal.pone.0117077

58. Quintelas, C., Rocha, Z., Silva, B., Fonseca, B., Figueiredo, H. & Tavares, T. (2009). Removal of Cd(II), Cr(VI), Fe(III) and Ni(II) from aqueous solutions by an E. coli biofilm supported on kaolin. *Chem. Eng. J.* 149, 319–324. DOI: 10.1016/j.cej.2008.11.025.

59. Karthikeyan, G. & Siva Ilango, S. (2008). Equilibrium Sorption studies of Fe, Cu and Co ions in aqueous medium using activated Carbon prepared from Recinius Communis Linn. *J. Appl. Sci. Environ. Manage.* 12(2), 81–87. http://dx.doi.org/10.4314/jasem.v12i2.55537

60. Ahalya, N., Kanamadi, R.D. & Ramachandra, T.V. (2007). Cr (VI) and Fe (III) removal using Cajanus cajan husk. *J. Environ. Biol.* 28(4), 765–769.

61. Dai, J., Ren, F.L. & Tao, C.Y. (2012). Adsorption Behavior of Fe(II) and Fe(III) Ions on Thiourea Cross-Linked Chitosan with Fe(III) as Template. *Molecules* 17, 4388–4399. DOI: 10.3390/molecules17044388.

62. Sankar, K.R., Venkatraman, B.R. & Arivoli, S. (2013). Equilibrium and Thermodynamics Studies on the Removal of Iron (III) onto Plaster of Paris. *Int. J. Eng. Innov. Res.* 2(1), 28–33.

63. Moradi, O., Zare, K. & Yari, M. (2011). Interaction of some heavy metal ions with single walled carbon nanotube. *Int. J. Nano. Dim.* 1(3), 203–220.

64. Salam, M.A., Makki, M.S.I. & Abdelaal, M.Y.A. (2011). Preparation and characterization of multi-walled carbon nanotubes/chitosan nanocomposite and its application for the removal of heavy metals from aqueous solution. *J. Alloys Compd.* 509, 2582–2587. DOI: 10.1016/j.jallcom.2010.11.094.

65. Unlu, N. & Ersoz, M. (2007). Removal of heavy metal ions by using dithiocarbamated-sporopollenin. *Sep. Purif. Technol.* 52, 461–469. DOI: 10.1016/j.seppur.2006.05.026.

66. Abdus-Salam, N. & Bello, M.O. (2015). Kinetics, thermodynamics and competitive adsorption of lead and zinc ions onto termite mound. *Int. J. Environ. Sci. Technol.* 12, 3417–3426. DOI: 10.1007/s13762-015-0769-2.

67. Salam, M.A. (2013). Removal of heavy metal ions from aqueous solutions with multi-walled carbon nanotubes: Kinetic and thermodynamic studies. *Int. J. Environ. Sci. Technol.* 10, 677–688. DOI: 10.1007/s13762-012-0127-6.

68. Kara, M., Yuzer, H., Sabah, E. & Celik, M.S. (2003). Adsorption of cobalt from aqueous solutions onto sepiolite. *Water Res.* 37, 224–232. http://dx.doi.org/10.1016/S0043-1354(02)00265-8

69. Jaycock, M.J. & Parfitt, G.D. (1981). *Chemistry of Interfaces.* Ellis Horwood Ltd., Onichester.